

# Joint Demosaicing and Arbitrary-Ratio Resizing Algorithm for Bayer Color Filter Array Based on DCT Approach

Kuo-Liang Chung<sup>a,\*</sup>, Wei-Jen Yang<sup>b</sup>, Mei-Ju Chen<sup>a</sup>, Wen-Ming Yan<sup>b</sup>, and Chiou-Shann Fuh<sup>b</sup>

<sup>a</sup>Department of Computer Science and Information Engineering

National Taiwan University of Science and Technology, Taipei, Taiwan R. O. C.

{k.l.chung, M9715007}@mail.ntust.edu.tw.

<sup>b</sup>Department of Computer Science and Information Engineering

National Taiwan University, Taipei, Taiwan R. O. C.

{f93035, ganboon, fuh}@csie.ntu.edu.tw.

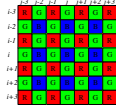


Figure 1: The Bayer CFA structure.

## Abstract

This paper presents a new joint demosaicing and arbitrary-ratio resizing algorithm for mosaic images. By using the adaptive heterogeneity projection masks and Sobel- and luminance estimation-based masks, the extracted edge information is utilized to construct the fully populated green color plane, green-red color difference plane, and green-blue color difference plane. Then, based on the composite cosine transform (DCT) technique, the above three constructed planes are resized to the arbitrary sized ones. Further, the resized red and blue color planes are constructed. Based on twenty-four popular testing mosaic images, the proposed resizing algorithm has better image quality performance when compared with two native algorithms.

**Keywords:** *Arbitrary-ratio resizing algorithm, Color difference, Color filter array, DCT, Demosaicing algorithm, Digital cameras.*

## 1. INTRODUCTION

Most digital cameras use a single sensor array to capture the color information based on Bayer color filter array (CFA) structure [1] which is depicted in Figure 1. In Bayer CFA structure, each pixel in the captured image has only one of the three primary colors and this kind of image is called the mosaic image. Because the green (G) color plane is the most important factor to determine the luminance of the color image, half of the pixels in Bayer CFA structure are assigned to G color plane; the red (R) and blue (B) color planes share the remaining parts evenly.

Since each pixel in the mosaic image has only one color components, the two missing color components for one color pixel should be recovered as best as possible and such a recovering process is called the demosaicing process which has been studied extensively [2, 3, 4, 5]. Besides the demosaicing issue, how to resize mosaic images is another important research issue. The terms “resize” and “zoom” are used exchangeably. Some resizing algorithms for mosaic images have been developed [6, 7]. Unfortunately, all of them

only focus on the quad-zooming process.

In this paper, a new joint demosaicing and arbitrary-ratio resizing algorithm for mosaic images is presented. Utilizing the the adaptive heterogeneity projection masks and the Sobel- and luminance estimation-based (SL-based) masks [4], the edge information can be extracted from the mosaic image directly and accurately. Then, based on the color difference concept and the composite length DCT [8], the mosaic image can be demosaiced and resized to obtain arbitrary-ratio sized full color images. Based on twenty-four popular testing mosaic images, the proposed algorithm has better image quality performance when compared with two native algorithms.

## 2. THE PROPOSED NEW JOINT DEMOSAICING AND ARBITRARY-RATIO RESIZING ALGORITHM FOR MOSAIC IMAGES

Before performing the proposed resizing algorithm, the tuned horizontal heterogeneity projection value  $HP'_H(i, j)$  and the tuned vertical heterogeneity projection values  $HP'_V(i, j)$  are computed by Adaptive heterogeneity projection, and then the horizontal gradient response  $\Delta I_{dm}^H(i, j)$ , the vertical gradient response  $\Delta I_{dm}^V(i, j)$ , the  $\frac{\pi}{4}$ -diagonal gradient response  $\Delta I_{dm}^{\frac{\pi}{4}}(i, j)$ , and the  $\frac{-\pi}{4}$ -diagonal gradient response  $\Delta I_{dm}^{\frac{-\pi}{4}}(i, j)$  are computed by SL-based masks [4]. Our proposed algorithm consists of the following three stages: (1) interpolating the mosaic G plane to construct the fully populated G plane by using the edge-sensing interpolation estimation; (2) interpolating the mosaic G-R and G-B color difference planes to construct the fully populated G-R and G-B color difference planes, respectively; (3) resizing the three constructed planes mentioned above to obtain the arbitrary-ratio size ones, and then based on the three resized planes, recovering the resized R and B planes to obtain arbitrary-ratio resized full color image.

### 2.1 Stage 1: Interpolating the mosaic G plane

In this subsection, the interpolation for the mosaic G plane  $I_{mo}^g$  to obtain the fully populated G plane  $I_{dm}^g$  by using the edge-sensing demosaicing algorithm is presented.

For exposition, let us take the central pixel at position  $(i, j)$  in Figure 1 as the representative to explain how to estimate the G color value  $I_{dm}^g(i, j)$  from its four neighboring pixels with movement  $\Omega_g = \{(x, y) | (x, y) = (i \pm 1, j), (i, j \pm 1)\}$ . First, according to the tuned horizontal heterogeneity projection value  $HP'_H(i, j)$  and vertical heterogeneity projection value  $HP'_V(i, j)$  of the current pixel, three cases, namely the horizontal variation as shown in Figure 2(a), the vertical variation as shown in Figure 2(b), and the other variations as shown in Figure 2(c), are considered in the interpolation estimation phase for  $I_{mo}^g(i, j)$ . The arrows in Figure 2

\*Corresponding author. Supported by the National Science Council of R. O. C. under contracts NSC98-2221-E-011-102-MY3 and NSC98-2923-E-011-001.

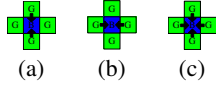


**Figure 2:** Data dependence of our proposed interpolation estimation for  $I_{mo}^g(i, j)$ . (a) Horizontal variation (vertical edge). (b) Vertical variation (horizontal edge). (c) The other variations.

denote the relevant data dependence.

Further, in order to estimate  $I_{dm}^g(i, j)$  more accurately, four proper weights in terms of the gradient magnitude are assigned to the corresponding four pixels in the interpolation estimation phase. Considering the neighboring pixel located at position  $(i-1, j)$ , if the vertical gradient magnitude is large, i.e. there is a horizontal edge passing through it, based on the color difference assumption [5], it reveals that the G component of this pixel makes less contribution to estimate that of the current pixel; otherwise, it reveals that the G component of this pixel makes more contribution to estimate that of the current pixel. According to the above analysis, the weight of the pixel at position  $(i-1, j)$  is given by  $w_g(V, i-1, j) = \frac{1}{1+\Delta I_{dm}^V(i-2, j)+2\Delta I_{dm}^V(i-1, j)+\Delta I_{dm}^V(i, j)}$ . By the same argument, the weights of the other three neighbors are determined by  $w_g(V, i+1, j) = \frac{1}{1+\sum_{k=0}^2 \delta_k \Delta I_{dm}^V(i+k, j)}$ ,  $w_g(H, i, j-1) = \frac{1}{1+\sum_{k=0}^2 \delta_k \Delta I_{dm}^H(i, j-k)}$ ,  $w_g(H, i, j+1) = \frac{1}{1+\sum_{k=0}^2 \delta_k \Delta I_{dm}^H(i, j+k)}$ , respectively, where  $\delta_k = 2$  if  $k = 1$ ;  $\delta_k = 1$ , otherwise. Consequently, the value of  $I_{dm}^g(i, j)$  can be estimated by

$$I_{dm}^g(i, j) = I_{mo}^b(i, j) + \frac{\sum_{(d, x, y) \in \xi_g} w_g(d, x, y) D_{gb}(x, y)}{\sum_{(d, x, y) \in \xi_g} w_g(d, x, y)}$$

$$\xi_g = \begin{cases} \xi_1 & \text{if } H P_V'(i, j) < \alpha H P_H'(i, j) \\ \xi_2 & \text{if } H P_H'(i, j) < \alpha H P_V'(i, j) \\ \xi_1 \cup \xi_2 & \text{otherwise} \end{cases}$$

where  $\xi_1 = \{(V, i \pm 1, j)\}$  and  $\xi_2 = \{(H, i, j \pm 1)\}$ ; for  $(d_1, x_1, y_1) \in \xi_1$ ,  $D_{gb}(x_1, y_1) = I_{mo}^g(x_1, y_1) - \frac{1}{2} \sum_{k \in \{\pm 1\}} I_{mo}^b(x_1 + k, y_1)$ ; for  $(d_2, x_2, y_2) \in \xi_2$ ,  $D_{gb}(x_2, y_2) = I_{mo}^g(x_2, y_2) - \frac{1}{2} \sum_{k \in \{\pm 1\}} I_{mo}^b(x_2, y_2 + k)$ ; the parameter  $\alpha$  is set to  $\alpha = 0.55$  empirically.

Finally, the refinement approach, which combines the concepts of the local color ratios [4] and the proper weighting scheme based on the gradient magnitude, is used to refine the fully populated G plane. For the current pixel at position  $(i, j)$ , its G value  $I_{dm}^g(i, j)$  can be refined by the following rule:

$$I_{dm}^g(i, j) = -\beta + (I_{mo}^b(i, j) + \beta) \frac{\sum_{(d, x, y) \in \xi_g'} \delta_{(d, x, y)} w_g(d, x, y) R_{gb}(x, y)}{\sum_{(d, x, y) \in \xi_g'} \delta_{(d, x, y)} w_g(d, x, y)}$$

where  $\xi_g' = \{(H, i, j), (V, i, j), (H, i, j \pm 1), (V, i \pm 1, j)\}$ ;  $R_{gb}(x, y) = \frac{I_{dm}^g(x, y) + \beta}{I_{mo}^b(x, y) + \beta}$ ;  $\delta_{(d, x, y)} = \frac{1}{2}$  if  $(d, x, y) \in \{(H, i, j), (V, i, j)\}$ ;  $\delta_{(d, x, y)} = 1$ , otherwise; the parameter  $\beta$  is set to  $\beta = 256$  empirically.

After performing the above the edge-sensing interpolation estimation, the fully populated G plane can be constructed. In next subsection, the fully populated G plane will be used to assist the interpolation of the mosaic G-R and G-B color difference planes.

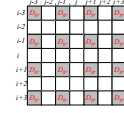


**Figure 3:** The pattern of the mosaic G-R color difference plane.

## 2.2 Stage 2: Interpolating the mosaic G-R and G-B color difference planes

Instead of interpolating the R and B color planes directly, we interpolate the G-R and G-B color difference planes because the color difference plane is much smoother than the original color plane and it would alleviate the amplification of the estimation error in the later resizing stage. Since the interpolation for G-R color difference plane is the same as that for G-B color difference plane, in what follows, we only present it for G-R color difference plane. Based on the mosaic image as show in Figure 1 and the fully populated G plane, the mosaic G-R plane can be obtained by  $D_{gr}(i_r, j_r) = I_{dm}^g(i_r, j_r) - I_{mo}^b(i_r, j_r)$ . Figure 3 illustrates the pattern of the obtained mosaic G-R color difference plane for the position depicted in gray cells.

The G-R color difference plane interpolation estimation for the other positions consists of the following two steps: Step 1: interpolating the G-R color difference values of the pixels at positions  $(i \pm 2m, j \pm 2n)$  in Fig. 6; Step 2: interpolating the G-R color difference values of the pixels at positions  $(i \pm 2m, j \pm 2n + 1)$  and  $(i \pm 2m + 1, j \pm 2n)$ . For simplicity, the central pixel at position  $(i, j)$  in Fig. 3 is taken as the representative to explain the G-R color difference plane interpolation in Step 1. Similar to the interpolation for the mosaic G plane mentioned in last subsection, the G-R color difference value  $D_{gr}(i, j)$  can be estimated from its four neighboring pixels with movement  $\Omega_r = \{(x, y) | (x, y) = (i \pm 1, j \pm 1)\}$ . In order to estimate  $D_{gr}(i, j)$  more accurately, the gradient magnitudes of four diagonal variations are considered to determine the proper four weights. Given a pixel at position  $(x, y)$ , its  $-\frac{\pi}{4}$ -diagonal and  $\frac{\pi}{4}$ -diagonal weights can be determined by  $w_{gr}(-\frac{\pi}{4}, x, y) = \frac{1}{1+\sum_{k=-1}^1 \delta_k \Delta I_{dm}^{-\frac{\pi}{4}}(i+k, j+k)}$  and  $w_{gr}(\frac{\pi}{4}, x, y) = \frac{1}{1+\sum_{k=-1}^1 \delta_k \Delta I_{dm}^{\frac{\pi}{4}}(i-k, j+k)}$ , respectively, where  $\delta_k = 2$  if  $k = 0$ ;  $\delta_k = 1$ , otherwise. Thus, the four weights of the four diagonal neighbors of the current pixel at position  $(i, j)$  are selected by  $w_{gr}(-\frac{\pi}{4}, i-1, j-1)$ ,  $w_{gr}(\frac{\pi}{4}, i-1, j+1)$ ,  $w_{gr}(\frac{\pi}{4}, i+1, j-1)$ , and  $w_{gr}(-\frac{\pi}{4}, i+1, j+1)$ , respectively. Based on the four weights, the G-R color difference value at position  $(i, j)$  can be estimated by

$$D_{gr}(i, j) = \frac{\sum_{(d, x, y) \in \xi_{gr}} w_{gr}(d, x, y) D_{gr}(x, y)}{\sum_{(d, x, y) \in \xi_{gr}} w_{gr}(d, x, y)}$$

where  $\xi_{gr} = \{(-\frac{\pi}{4}, i-1, j-1), (\frac{\pi}{4}, i-1, j+1), (\frac{\pi}{4}, i+1, j-1), (-\frac{\pi}{4}, i+1, j+1)\}$ .

After performing Step 1, the current pattern of the G-R color difference plane is illustrated in Fig. 4(a). For easy exposition, the central pixel at position  $(i', j')$  in Fig. 4(b), which is obtained by shifting Fig. 4(a) one pixel down, is taken as the representative to explain the G-R color difference plane interpolation in Step 2. Referring to Fig. 4(b), it is not hard to find that the pattern of the G-R color difference plane at present is the same as that of the G plane in the mosaic image as shown in Fig. 1. Therefore, the interpolation estimation approach described in last subsection can be directly used to estimate the G-R color difference value at position

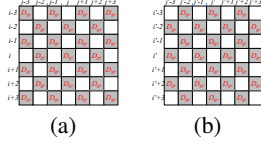


**Figure 4:** Two patterns of the G-R color difference plane. (a) The pattern of the G-R color difference plane after performing Step 1. (b) The pattern shifting (a) one pixel down.

$(i', j')$ . Consequently, the G-R color difference value of the current pixel can be estimated by

$$D_{gr}(i', j') = \frac{\sum_{(d,x,y) \in \xi'_{gr}} w_{gr}(d, x, y) D_{gr}(x, y)}{\sum_{(d,x,y) \in \xi'_{gr}} w_{gr}(d, x, y)}$$

$$\xi'_{gr} = \begin{cases} \xi_1 & \text{if } H P'_V(i', j') < \alpha H P'_H(i', j') \\ \xi_2 & \text{if } H P'_H(i', j') < \alpha H P'_V(i', j') \\ \xi_1 \cup \xi_2 & \text{otherwise} \end{cases}$$

where  $\xi_1 = \{(V, i' \pm 1, j')\}$  and  $\xi_2 = \{(H, i', j' \pm 1)\}$ ;  $w_{gr}(H, x, y) = \frac{1}{1 + \sum_{k=-1}^1 \delta_k \Delta I_{dm}^H(x, y+k)}$  and  $w_{gr}(V, x, y) = \frac{1}{1 + \sum_{k=-1}^1 \delta_k \Delta I_{dm}^V(x+k, y)}$  where  $\delta_k = 2$  if  $k = 0$ ;  $\delta_k = 1$ , otherwise; the parameter  $\alpha$  is set to  $\alpha = 0.55$  empirically.

After constructing the fully populated G plane, G-R color difference plane, and G-B color difference plane, in next subsection, the three constructed planes will be resized to the arbitrary-ratio sized ones, and then the arbitrary-ratio resided full color image is followed.

### 2.3 Stage 3: Resizing the three related planes

Based on the composite length DCT [8], this subsection presents the arbitrary-ratio resizing stage for the fully populated G plane  $I_{dm}^g$ , G-R color difference plane  $D_{gr}$ , and G-B color difference plane  $D_{gb}$ . Since the resizing stage for  $I_{dm}^g$  is the same as that for  $D_{gr}$  and  $D_{gb}$ , we only present it for  $I_{dm}^g$ . Let  $DCT(B^{(a)})$  and  $IDCT(B^{(a)})$  be the DCT and inverse DCT on the block  $a \times a$   $B^{(a)}$ . For the fully populated G plane  $I_{dm}^g$  with size  $M \times N$ , we first divide it into a set of the image blocks, each with size  $8 \times 8$ , and the obtained image block set is denoted by  $\Phi_{I_{dm}^g} = \{B_{m,n}^{(8)} | 0 \leq m \leq \frac{M}{8} - 1, 0 \leq n \leq \frac{N}{8} - 1\}$  where  $B_{m,n}^{(8)}$  denotes the  $(\frac{mN}{8} + n)$ -th block in  $\Phi_{I_{dm}^g}$ . Then, the DCT is performed on each  $8 \times 8$  image block  $\{B_{m,n}^{(8)}\}$  to obtain the set of transformed blocks,  $\hat{\Phi}_{I_{dm}^g} = \{\hat{B}_{m,n}^{(8)} | 0 \leq m \leq \frac{M}{8} - 1, 0 \leq n \leq \frac{N}{8} - 1\}$ . If we want to resize the  $M \times N$  G plane  $I_{dm}^g$  to the one with size  $\frac{q}{p}M \times \frac{q}{p}N$ , the resizing ratio is said to  $\frac{q}{p}$ . According to the resizing ratio  $\frac{q}{p}$ , first  $p^2$  blocks in  $\hat{\Phi}_{I_{dm}^g}$  are collected to be an active unit which are surrounded by dashed lines in Fig. 5. In order to achieve resizing ratio  $\frac{q}{p}$ , the  $p^2$  blocks in each active unit should be increased or decreased to  $q^2$  blocks.

For the active unit  $\hat{\Psi}_{Act} = \{\hat{B}_{m,n}^{(8)} | 0 \leq m, n \leq p - 1\}$ , the  $\frac{q}{p}$ -fold resizing procedure consists of the following four steps:

**Step 1:** Each  $8 \times 8$  DCT coefficient block  $\hat{B}_{m,n}^{(8)}$  in the active unit is expanded to a  $(8+z) \times (8+z)$  block  $\hat{B}'_{m,n}^{(8+z)}$  by the

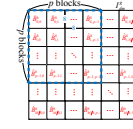


**Figure 5:** An example of the active unit in  $\hat{\Phi}_{I_{dm}^g}$ .

following zero padding rule:

$$\hat{B}'_{m,n}^{(8+z)}(x, y) = \begin{cases} \hat{B}_{m,n}^{(8)}(x, y) & \text{if } 0 \leq x, y < 8 \\ 0 & \text{otherwise} \end{cases}$$

$$\forall x, y \in \{0, 1, \dots, z-1\}; \forall m, n \in \{0, 1, \dots, p-1\}$$

where  $z$  denotes the smallest nonnegative integer satisfying the condition:  $p(8+z) = Cq$ ,  $C \geq 8$ . Consequently, we have the set of zero padded DCT coefficient blocks  $\hat{\Psi}'_{Act} = \{\hat{B}'_{m,n}^{(8+z)} | 0 \leq m, n \leq p-1\}$ .

**Step 2:** For each  $\hat{B}'_{m,n}^{(8+z)}$  in  $\hat{\Psi}'_{Act}$ , the  $(8+z) \times (8+z)$  IDCT is performed on it to obtain the upsized image:

$$B'_{m,n}^{(8+z)} = IDCT(\hat{B}'_{m,n}^{(8+z)}), \quad 0 \leq m, n \leq p-1.$$

After performing the  $(8+z) \times (8+z)$ -sample IDCT's on all the zero padded DCT coefficient blocks in  $\hat{\Psi}'_{Act}$ , the upsized subimage  $I_{up} (= \bigcup_{0 \leq m, n \leq p-1} B'_{m,n}^{(8+z)})$  is constructed.

**Step 3:** Then, the upsized subimage  $I_{up}$  is divided into  $q^2$  blocks, each block with size  $\frac{p}{q}(8+z) \times \frac{p}{q}(8+z)$ , and the set of the resampled image blocks is denoted by  $\Psi_{Re} = \{R_{m,n}^{(\frac{p}{q}(8+z))} | 0 \leq m, n \leq q-1\}$ . Next, the DCT is performed on each  $R_{m,n}^{(\frac{p}{q}(8+z))}$  in  $\Psi_{Re}$  to construct the resampled DCT coefficient block  $\hat{R}_{m,n}^{(\frac{p}{q}(8+z))}$

$$\hat{R}_{m,n}^{(\frac{p}{q}(8+z))} = DCT(R_{m,n}^{(\frac{p}{q}(8+z))}), \quad 0 \leq m, n \leq q-1.$$

We thus have the set of resampled DCT coefficient blocks  $\hat{\Psi}_{Re} = \{\hat{R}_{m,n}^{(\frac{p}{q}(8+z))} | 0 \leq m, n \leq q-1\}$ .

**Step 4:** Finally, the high-frequency DCT coefficients of each block in  $\hat{\Phi}_{Re}$  are truncated by the following rule:

$$\hat{R}'_{m,n}^{(8)}(x, y) = \hat{R}_{m,n}^{(\frac{p}{q}(8+z))}(x, y)$$

$$\forall x, y \in \{0, 1, \dots, 8\}; \forall m, n \in \{0, 1, \dots, q-1\}$$

where  $\hat{R}'_{m,n}^{(8)}$  denotes the left-upper  $8 \times 8$  subblock of  $\hat{R}_{m,n}^{(\frac{p}{q}(8+z))}$ ;  $\hat{R}_{m,n}^{(\frac{p}{q}(8+z))}(x, y)$  and  $\hat{R}'_{m,n}^{(8)}(x, y)$  denote the DCT coefficients of the pixels at position  $(x, y)$  in  $\hat{R}_{m,n}^{(\frac{p}{q}(8+z))}$  and  $\hat{R}'_{m,n}^{(8)}$ , respectively. Consequently, the resized active unit  $\hat{\Psi}'_{Re} = \{\hat{R}'_{m,n}^{(8)} | 0 \leq m, n \leq q-1\}$  is constructed.

After performing the above resizing procedure on all the active units in  $I_{dm}^g$ , the new set of the DCT coefficient blocks  $\hat{\Phi}_{Z_{dm}^g} = \{\hat{B}'_{m,n}^{(8)} | 0 \leq m \leq \frac{q}{p}M - 1, 0 \leq n \leq \frac{q}{p}N - 1\}$  can be obtained. Consequently, the  $\frac{q}{p}M \times \frac{q}{p}N$  sized G plane  $Z_{dm}^g$  can be obtained by performing the  $8 \times 8$ -sample IDCT on all the DCT coefficient



**Figure 6:** The twenty-four testing images from Kodak PhotoCD.

**Table 1:** Average CPSNR comparison for the three concerned algorithms.

|       | CPSNR         |               |              | $\Delta E_{ab}^*$ |               |               |         |
|-------|---------------|---------------|--------------|-------------------|---------------|---------------|---------|
|       | $\frac{q}{p}$ |               | Average      | $\frac{q}{p}$     |               |               | Average |
|       | 2             | $\frac{4}{3}$ |              | 2                 | $\frac{4}{3}$ | $\frac{4}{3}$ |         |
| $A_1$ | 28.41         | 32.16         | 30.29        | 3.529             | 2.624         | 3.077         |         |
| $A_2$ | 28.61         | 32.57         | 30.34        | 3.416             | 2.503         | 2.960         |         |
| Ours  | <b>29.12</b>  | <b>33.58</b>  | <b>31.35</b> | <b>3.194</b>      | <b>2.342</b>  | <b>2.718</b>  |         |

blocks in  $\hat{\Phi}_{Z_{dm}^g}$ . By the same argument, the resized G-R and G-B color difference planes,  $ZD_{gr}$  and  $ZD_{gb}$ , can be also obtained. Finally, the resized R and B planes can be constructed by

$$\begin{aligned} Z_{dm}^r(i_z, j_z) &= Z_{dm}^g(i_z, j_z) - ZD_{gr}(i_z, j_z) \\ Z_{dm}^b(i_z, j_z) &= Z_{dm}^g(i_z, j_z) - ZD_{gb}(i_z, j_z) \\ \forall i_z \in \{0, 1, \dots, \frac{q}{p}M - 1\}, \forall j_z \in \{0, 1, \dots, \frac{q}{p}N - 1\} \end{aligned}$$

where  $Z_{dm}^r(i_z, j_z)$ ,  $Z_{dm}^g(i_z, j_z)$ , and  $Z_{dm}^b(i_z, j_z)$  denote the three color components of the pixel at position  $(i_z, j_z)$  in the resized full color image  $Z_{dm}$ , respectively;  $ZD_{gr}(i_z, j_z)$  and  $ZD_{gb}(i_z, j_z)$  denote the G-R and G-B color difference value of the pixel at position  $(i_z, j_z)$  in  $ZD_{gr}$  and  $ZD_{gb}$ , respectively.

### 3. EXPERIMENTAL RESULTS

In this section, based on twenty-four popular testing mosaic images, some experimental results are demonstrated to show the applicability and quality advantages of the proposed algorithm. Fig. 6 illustrates the twenty-four testing images from Kodak PhotoCD. In our experiments, the twenty-four testing images, each with size  $512 \times 728$ , are first downsized to the  $\frac{p}{q} \cdot 512 \times \frac{p}{q} \cdot 728$  sized ones, and then the downsized images are down-sampled to the mosaic images.

In the two native resizing algorithms to be compared with our proposed algorithm, one of the two demosaicing methods proposed in [5] and [3], respectively, is first utilized to obtain the demosaiced images and then the resizing method proposed in [8] is applied to construct the resized full color images. For convenience, the three native algorithms based on the demosaicing methods proposed in [5] and [3] are called  $A_1$  and  $A_2$ , respectively.

Here, we adopt two objective color image quality measures, the CPSNR and the S-CIELAB  $\Delta E_{ab}^*$  [4], and one subjective color image quality measure, the color artifacts, to justify the the quality advantage of the proposed algorithm. Based on the twenty-four testing images, among the four algorithms, Table 1 demonstrates the image quality comparison in terms of the average CPSNR and the average S-CIELAB  $\Delta E_{ab}^*$ , respectively. From Table 1, it is observed that the proposed resizing algorithm produces the best image quality in terms of CPSNR and S-CIELAB  $\Delta E_{ab}^*$ .

Next, the subjective image visual measure, color artifacts, is adopted to demonstrate the visual quality advantage of the proposed resizing algorithm. For saving space, we just show the visual com-



**Figure 7:** For image No. 23, when the resizing ratio  $\frac{q}{p}$  is  $\frac{4}{3}$ , four magnified subimages cut from the resized images obtained by (a) original image, (b)  $A_1$ , (c)  $A_2$ , and (d) the proposed algorithm.

parison when the resizing ratio  $\frac{q}{p}$  is  $\frac{4}{3}$ . Four magnified subimages cut from the testing image No. 23 are adopted to examine the visual effect among the three concerned algorithms. Figures 7 (a)–(d) illustrate magnified subimages cut from the resized images obtained by original image and the three concerned resized algorithms, respectively. From the visual comparison, it is observed that based on the same resizing ratio, the proposed algorithm produces less color artifacts when compared with the other two algorithms.

### 4. CONCLUSIONS

In this paper, a new joint demosaicing and arbitrary-ratio resizing algorithm for mosaic images has been presented. Based on the color difference concept and the composite length DCT, the mosaic image can be demosaiced and resized to the arbitrary-ratio sized full color image. Based on twenty-four popular testing mosaic images, the proposed new resizing algorithm has better image quality performance when compared with three native algorithms.

### 5. REFERENCES

- [1] B. E. Bayer, "Color imaging array," *U.S. Patent# 3 971 065*, 1976.
- [2] H. A. Chang and H. H. Chen, "Stochastic color interpolation for digital cameras," *IEEE Trans. Circuits and Systems for Video Technology*, vol. 17, no. 8, pp. 964–973, 2007.
- [3] K. H. Chung and Y. H. Chan, "Color demosaicking using variance of color differences," *IEEE Trans. Image Processing*, vol. 15, no. 10, pp. 2944–2955, 2006.
- [4] K. L. Chung W. J. Yang W. M. Yan and C. C. Wang, "Demosaicing of color filter array captured images using gradient edge detection masks and adaptive heterogeneity-projection," *IEEE Trans. Image Processing*, vol. 17, no. 12, pp. 2356–2367, 2008.
- [5] S. C. Pei and I. K. Tam, "Effective color interpolation in ccd color filter arrays using signal correlation," *IEEE Trans. Circuits and Systems for Video Technology*, vol. 13, no. 6, pp. 503–513, 2003.
- [6] R. Lukac K. N. Plataniotis and D. Hatzinakos, "Color image zooming on the bayer pattern," *IEEE Trans. Circuits and Systems for Video Technology*, vol. 15, no. 11, pp. 1475–1492, 2005.
- [7] L. Zhang and D. Zhang, "A joint demosaicking-zooming scheme for single chip digital color cameras," *Computer Vision and Image Understanding*, vol. 107, no. 1-2, pp. 14–25, 2009.
- [8] Y. S. Park and H. W. Park, "Arbitrary-ratio image resizing using fast dct of composite length for dct-based transcoder," *IEEE Trans. Image Processing*, vol. 15, no. 2, pp. 494–500, 2006.